Supplementary Information

Exploring the optimal posttreatment strategy for boosting the electrochemical performances of a new bimetal–organic framework-based supercapacitor

Xinwen Dou, Mingyue Liu, Tian Cao, Chan Wang, Yingjie Zhang, Yuhang Jia, Qiang Ju and Zhenlan Fang*

Table of Contents

1.0 Experimental part: synthesis and characterizations

1.1 Materials

Carbon cloth (CC) was purchased from Shanghai Hesen Co., Ltd.; Ethanol (99.7%) and *N*, *N*-dimethylformamide (DMF, ≥99.5%) were purchased from Wuxi Yasheng Chemical Co., Ltd.; $Ni(NO_3)_2·6H_2O$ (98%), 1,4-dicarboxybenzene (BDC, 96%), $Na_2S·9H_2O$(96%), carbon black (≥99.9%), polyvinylidene fluoride (PVDF, ≥99.9%) and N-methylpyrrolidone (NMP, 99.9%) were purchased from Energy-Chemical, Anhui Zesheng Technology Co., Ltd.; $Co(NO_3)_2·6H_2O$ (98.5%) was purchased from Sinopharm Chemical Reagent Co., Ltd.; polypyrrole (98%) and KOH (95.0%) were purchased from Shanghai Macklin Biochemical Co., Ltd.; NaCl (≥99.5%) was purchased from Guangzhou Xilong Chemical Reagent Co., Ltd.; Ethylene glycol (EG, ≥99.0%), H_2SO_4 (95-98 wt%) and $KMnO_4$ (99.5%) were purchased from Shanghai Lingfeng Chemical Reagent Co., Ltd., and all these chemical reagents were used without further purification.

1.2 Methods

Synthesis of Ni_xCo_y-MOF: In a typical synthesis of Ni_xCo_y-MOF, a mixture of 0.9 mmol 1,4-dicarboxybenzene (BDC) and 2.5 mmol $M(NO_3)_2·6H_2O$ (M = Ni, Co and the mixture of Ni and Co with feeding ratio of 2:1, 1:1 and 1:2, respectively) was dissolved in a mixed solution of DMF (8 mL) and EG (5 mL). After stirred for 0.5 h, the mixture was transferred to a Teflon-lined autoclave (20 mL), heated at 180 °C for 8 h before cooling down to room temperature with a rate of 30 ˚C h^{-1}. After centrifugation at 8000 rpm/min for 4 minutes and sequentially washing with DMF and anhydrous ethanol several times to remove unreacted chemical reagents, the precipitate was finally dried at 60 ˚C for 12 h. The detailed experimental conditions are listed in Table S1.

Synthesis of Ni_xCo_y-S: Ni/Co-S was prepared by dissolving of Ni_xCo_y-MOF (80 mg) in ethanol (7 mL) with ultrasonication for 1 h, followed by stirring for 30 min. In another breaker, 40 mg of $Na_2S·9H_2O$ was added to deionized water (7 mL) and stirred for 20 min. Next, the two solutions were mixed, and the mixture was stirred for 3 min. The mixture was then placed in a 25 mL Teflon-lined stainless autoclave, and kept at 140 °C for 6 h, and then cooled to room temperature. After

centrifugation, the obtained Ni_xCo_y-S powder products were washed with ethanol and deionized water alternately, and then dried at 70 °C overnight.

Synthesis of Ni_2Co_1-C: Ni_2Co_1-C was prepared by heating Ni_2Co_1-MOF (100 mg) to 600℃ at a rate of 5℃/min under an Ar flow, and then kept at 600℃ for 6 h.

Synthesis of Ni_2Co_1-O: Ni_2Co_1-O was prepared by heating Ni_2Co_1-MOF (100 mg) to 250℃ at a rate of 5℃/min under air, and then kept at 600℃ for 6 h.

Synthesis of Ni_2Co_1-OH: Ni_2Co_1-OH was prepared by immersing of Ni_2Co_1-MOF (100 mg) in 1 M KOH under stirring for 6 h at room temperature. After that, the solid was separated by deionized water and ethanol to remove the redundant KOH.

Table. S1 The detailed synthesis parameters of a series of Ni_xCo_y-MOF samples

Sample	$Ni(NO_3)_2$ ·$6H_2O$ (g/mmol)	$Co(NO_3)_2$ ·$6H_2O$ (g/mmol)	BDC (g/mmol)	EG (mL)	DMF (mL)	Temperature (℃)	Time (h)
Ni-MOF	0.75/2.5mmol	0/0	0.15/0.9mmol	25	40	180	8
Co-MOF	0/0	0.75/2.5 mmol	0.15/0.9mmol	25	40	180	8
Ni_1Co_2-MOF	0.25/0.83mmol	0.5/1.66 mmol	0.15/0.9mmol	25	40	180	8
Ni_1Co_1-MOF	0.37/1.25mmol	0.37/1.25mmol	0.15/0.9mmol	25	40	180	8
Ni_2Co_1-MOF	0.5/1.66mmol	0.25/0.83mmol	0.15/0.9mmol	25	40	180	8

Synthesis of acid-etched carbon cloth (AECC): The 1 × 1 cm^2 CC pieces were immersed in a mixed solvent of 10 ml HNO_3 (65-68 wt%) and 20 ml H_2SO_4 (95-98 wt%), which was sealed in Teflon-lined autoclave (50 mL), and then heated at 60 ˚C for 2 h. After cooling to room temperature, 1.5 g $KMnO_4$ was slowly added to the above solvent, and the CC pieces were kept in it for another 18 h, followed by adding 100 mL deionized water and 3 mL H_2O_2 to the resulting solution. The treated CC was washed repeatedly with deionized water under ultrasonication for 2 h, and finally dried at 60 ˚C to yield the final product AECC.

Electrodeposition of PPy on AECC (PPy@AECC): An electrochemical workstation (CHI660E) was used to electrodeposit PPy film on the AECC electrode with the 1 × 1 cm^2 working area, and the

AECC, Ag/AgCl and Pt foil were used as working electrode, reference electrode and counter electrode, respectively. The electrolyte was prepared by dissolving 0.135 g pyrrole and 0.235 g NaCl into 30 mL deionized water. The PPy@AECC cathode with PPy ranging from 3 to 6 mg cm^{-2} was obtained through electrodeposition of PPy on AECC at a constant potential of 1.0 V for 1000 s.

1.3 Characterization methods

Material characterization: Powder X-ray diffraction (PXRD) patterns of all samples were recorded on a Rigaku Smartlab (3 KW) equipment with a Ni filter using Cu-Kα radiation (λ = 1.542 Å). The patterns were collected in reflectance of Bragg-Brentano geometry over a range of 2θ = 5° – 50° at room temperature. Fourier transform infrared spectrum (FTIR) patterns of all samples were recorded using a Bruker ALPHA FTIR under nitrogen atmosphere in the range 4000 – 400 cm^{-1}, placed in a N_2 glove-box. X-ray photoelectron spectroscopy (XPS) analysis was carried out on a Thermo Scientific ESCALAB 250 Xi spectrometer with a monochromatized Al Kα X-ray source (1486.6 eV) at a constant dwell time of 50 ms and a pass-energy of 50 eV. The binding energies were calibrated to the C 1s line at 284.8 eV as a reference, and the XPS spectra were deconvoluted using the software Avantage. N_2 adsorption/desorption measurements: the BET surface areas and pore size distributions, were determined from the isothermal N_2 (99.9999%) adsorption/desorption curves of all samples with weight of ~100 mg, recorded by the Micromeritics 3 FLEX instrument at 78 K, and analyzed by both Barrett-Joyner-Halenda (BJH) and Density Functional Theory (DFT) methods. The Ni_2Co_1-MOF was immersed in ethanol at 80 °C for 24 h, then dried in an oven at 80 °C under air for 12 h, all obtained samples were activated at 180 °C under vacuum (~10^{-3} mbar) for 24 h. The morphologies and chemical compositions of all samples were investigated by a JSM 7800F scanning electron microscope (SEM) equipped with an energy dispersive X-ray spectrum (EDS). Transmission electron microscope (TEM) was performed by a Talos JEM-1400PLUS transmission electron microscope at an acceleration voltage of 200 kV.

Electrochemical Measurement: The electrochemical performances of the prepared working electrodes were carried out in 1.0 M KOH electrolyte using a CHI660E electrochemical workstation (Chenhua Instrument Co., Ltd., Shanghai, China) with a three-electrode system: a platinum plate as

the counter electrode and Ag/AgCl as the reference electrode. For the working electrode, active materials (80%), carbon black (10%) and polyvinylidene fluoride (PVDF, 10%) were mixed into the *N*-methylpyrrolidone (NMP), afterword a piece of nickel foam (1 cm × 1 cm) was immersed in the resulting homogeneous slurry, followed by being heated at 80 °C for 12 h and subsequently pressed under 10.0 MPa. The electrochemical tests for the as-prepared working electrode were examined by cyclic voltammetry (CV) and galvanostatic charge/discharge (GCD). Electrochemical impedance spectroscopy (EIS) was conducted in a frequency range from 0.01 to 10^5 Hz, while the cycle performance was measured using a NEWARE CT-4008T-5V-50mA-164 (Neware Co., Ltd., China) battery testing system.

Aqueous asymmetric supercapacitors (A-ASC) were assembled by Ni_2Co_1-S based positive electrodes and PPy@AECC negative electrodes in 1.0 M KOH aqueous solution electrolyte.

The specific capacitance was determined by following Eq. 1:

$$C = \frac{I\Delta t}{m\Delta V} \quad \text{……Eq. 1}$$

in which C (F g^{-1}), m (g), I (A), Δt (s) and ΔV (V) represent for specific capacitance, mass of active material in one electrode, charge/discharge current, discharge time and potential window, respectively.

The energy density (E, Wh kg^{-1}) and power density (P, W kg^{-1}) of the A-ASC were calculated by Eq. 2 and Eq. 3, respectively.

$$E = \frac{1}{2} \times \frac{C}{3600}(\Delta V)^2 \quad \text{……Eq. 2}$$

$$P = \frac{3600 \times E}{\Delta t} \quad \text{…… Eq. 3}$$

Herein, C is specific capacitance of the A-ASC, calculated by the weight sum of active materials in both positive and negative electrode; ΔV (V) and Δt (s) represent the voltage window and discharge time of the A-ASC, respectively.

Supplementary Tab. S2 Ratio of Ni^{3+} to Ni^{2+}, Co^{3+} to Co^{2+}, Ni to Co, M^{3+} to M^{2+}

	[a]Ratio of Ni to Co	[b]Ratio of Ni^{3+} to Ni^{2+}	[b]Ratio of Co^{3+} to Co^{2+}	[b]Ratio of M^{3+} to M^{2+}
Ni_1Co_1-MOF	0.96			
Ni_1Co_2-MOF	0.49			
Ni_2Co_1-MOF	1.82	0.46	2.26	0.90
Ni_2Co_1-S-140-6		0.62	2.46	1.54
Ni_2Co_1-C		1.50	1.85	1.68
Ni_2Co_1-O		1.75	1.61	1.71
Ni_2Co_1-OH		0.47	2.56	0.82

[a] Ratio of Ni to Co is determined by ICP-OES elemental analysis.

[b] Ratio of Ni to Co is determined by XPS analysis

Supplementary Tab. S3. BET surface areas and total pore volumes of all the dried samples. All the calculations are based on their N_2 sorption isotherms at 78 K.

	BET [m^2/g]	Total pore volume (p/p0 = 0.95) [cm^3/g]
Ni_2Co_1-MOF	747.88	0.606
Ni_2Co_1-S-140-6	63.77	0.140
Ni_2Co_1-C	59.73	0.104
Ni_2Co_1-O	24.22	0.041
Ni_2Co_1-OH	154.24	0.253

1.4 Thermogravimetric analysis

1.4.1 TGA curves of Ni_xCo_y-MOF

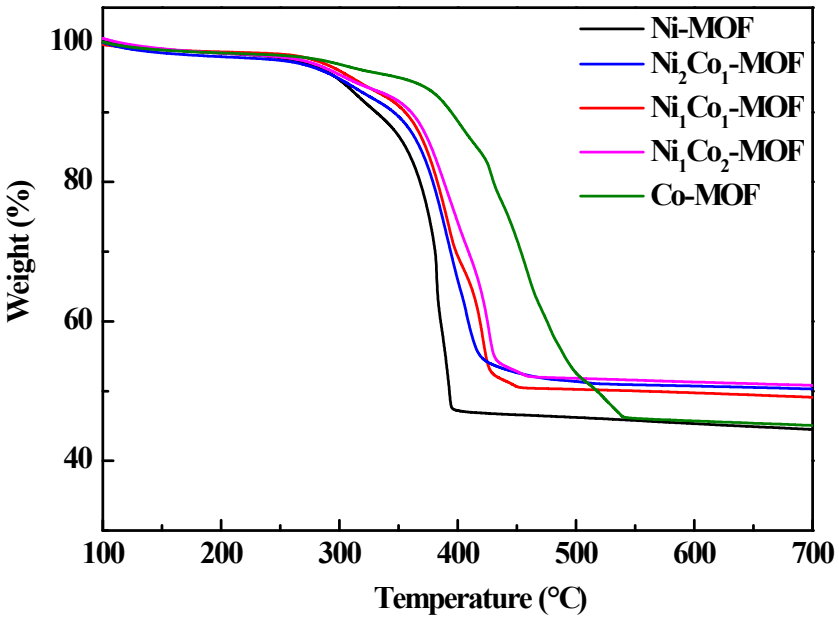

Fig. S1 TGA curves of dry Ni_xCo_y-MOFs ($x = 1$, $y = 0$; $x = 2$, $y = 1$; $x = 1$, $y = 1$; $x = 1$, $y = 2$; $x = 0$, $y = 1$) samples after removal of guest molecules by heat treatment at 180 ℃ for 12 hours under nitrogen.

The TGA curves of the dry Ni_xCo_y-MOFs samples under nitrogen, obtained after removing all solvent molecules, show that the thermostability stability of them are elevated along with increasing the content of Co ion, being consistent with that of as-synthesized ones (Fig. S1). The mass loss in the temperature range from 250 ℃ to 550 ℃ of monometallic Ni_xCo_y-MOFs (54.1%), assigned to the decomposition of main skeleton due to the dissociation of BDC ligand, is obviously higher than that of bimetallic Ni_xCo_y-MOFs (48.43%−49.95%), probably attributed to the missing ligand defects due to the competition of Ni and Co ions coordinating to BDC ligand.[1-4]

1.5 SEM analysis

1.5.1 SEM images of Ni_xCo_y-S-140-6 ($x = 1, y = 0$; $x = 1, y = 1$; $x = 1, y = 2$; $x = 0, y = 1$)

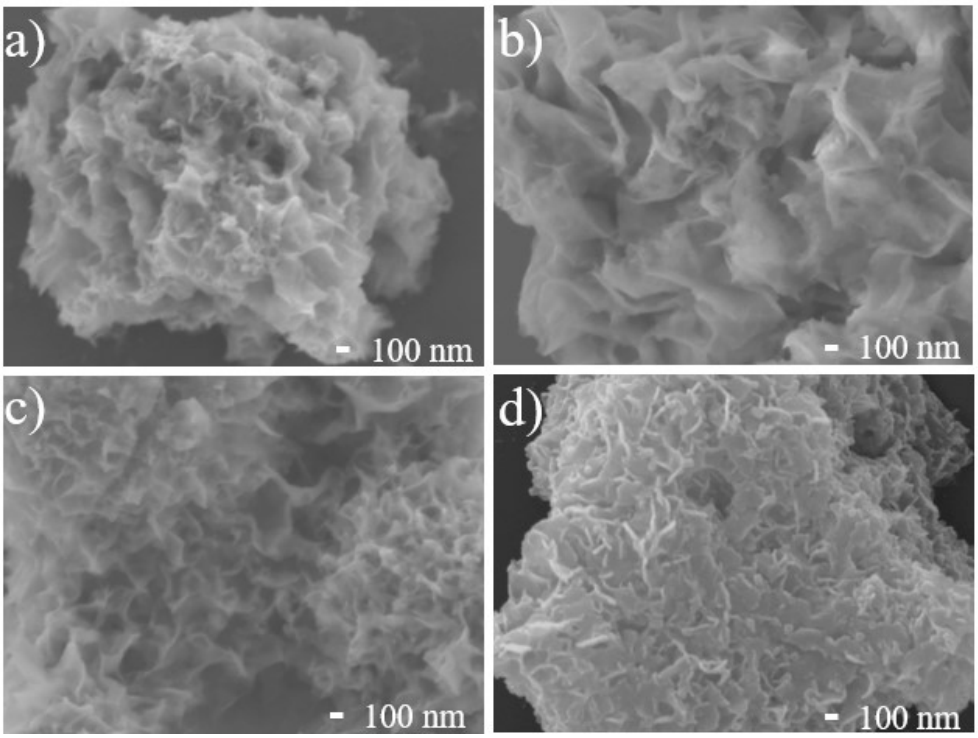

Fig. S2 The SEM images of (a) Ni-S-140-6, (b) Ni_1Co_1-S-140-6, (c) Ni_1Co_2-S-140-6, and (d) Co-S-140-6.

All the sulfides derived from monometallic and bimetallic Ni_xCo_y-MOFs after sulfidation at 140 ℃ for 6 h exhibit the tremella-like morphology, assembled by abound nanosheets. The looseness degree and sizes of interlaced nanosheets firstly increase when the content of Co ions from 0 to 50%, and then decrease along with increasing the content of Co ions up to 100%. The incorporation of Co ions in the Ni-MOFs leads to slightly modification on the morphology of their respective sulfides, further illustrating the good compatibility of cobalt and nickel ions in the framework of MOFs.

1.5.2 SEM images of Ni_xCo_y-MOF, Ni_2Co_1-C, Ni_2Co_1-O, Ni_2Co_1-OH, and Ni_2Co_1-S-140-6

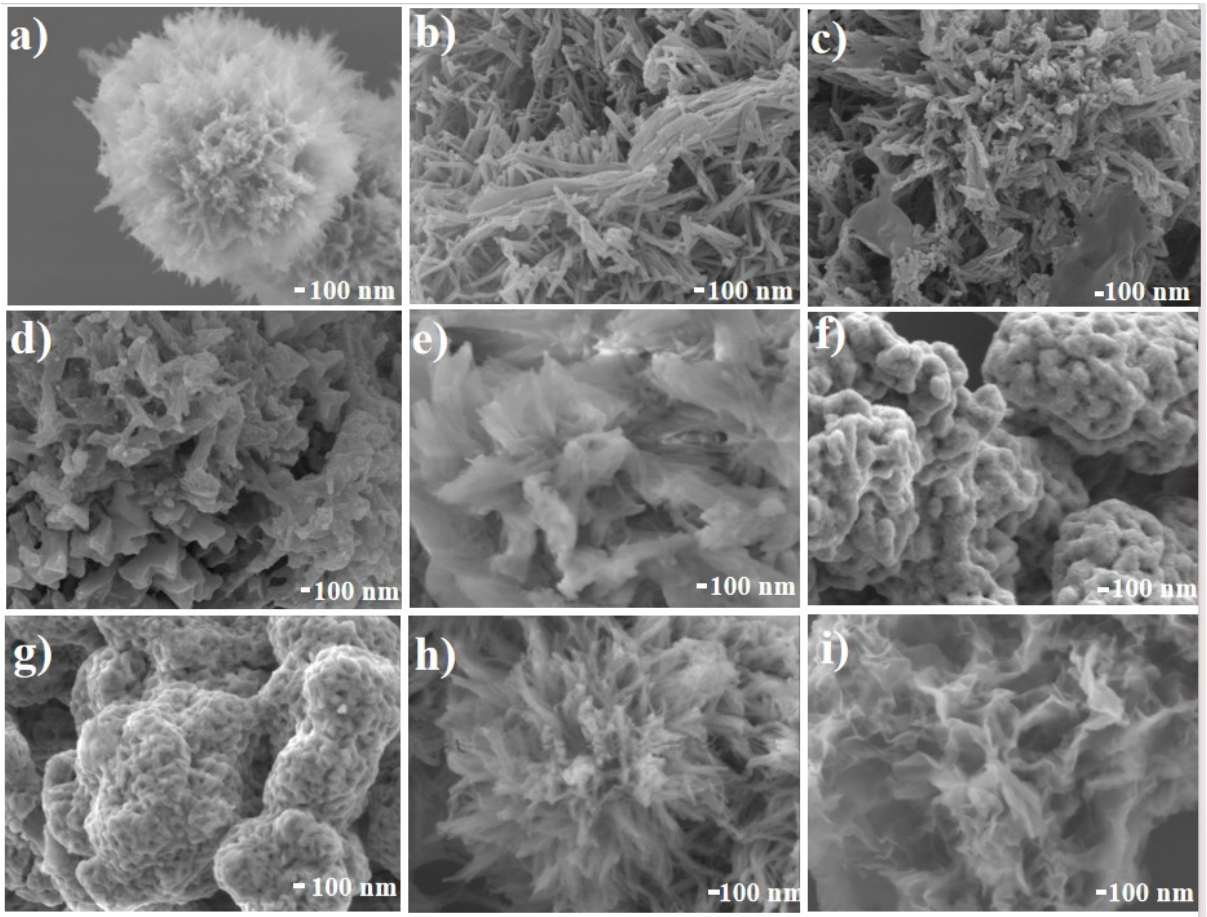

Fig. S3 The SEM images of (a) Ni-MOF, (b) Ni_2Co_1-MOF, (c) Ni_1Co_1-MOF, (d) Ni_1Co_2-MOF, (e) Co-MOF, (f) Ni_2Co_1-C, (g) Ni_2Co_1-O, (h) Ni_2Co_1-OH, and (i) Ni_2Co_1-S-140-6.

The detailed discussions about the comparison of morphologies of Ni_xCo_y-MOF, Ni_2Co_1-C, Ni_2Co_1-O, Ni_2Co_1-OH, and Ni_2Co_1-S-140-6 have been described in the section of Scanning electron microscopy of main text.

1.5.3 SEM images of Ni_2Co_1-S-140-*t* (T=1, 6, 12h)

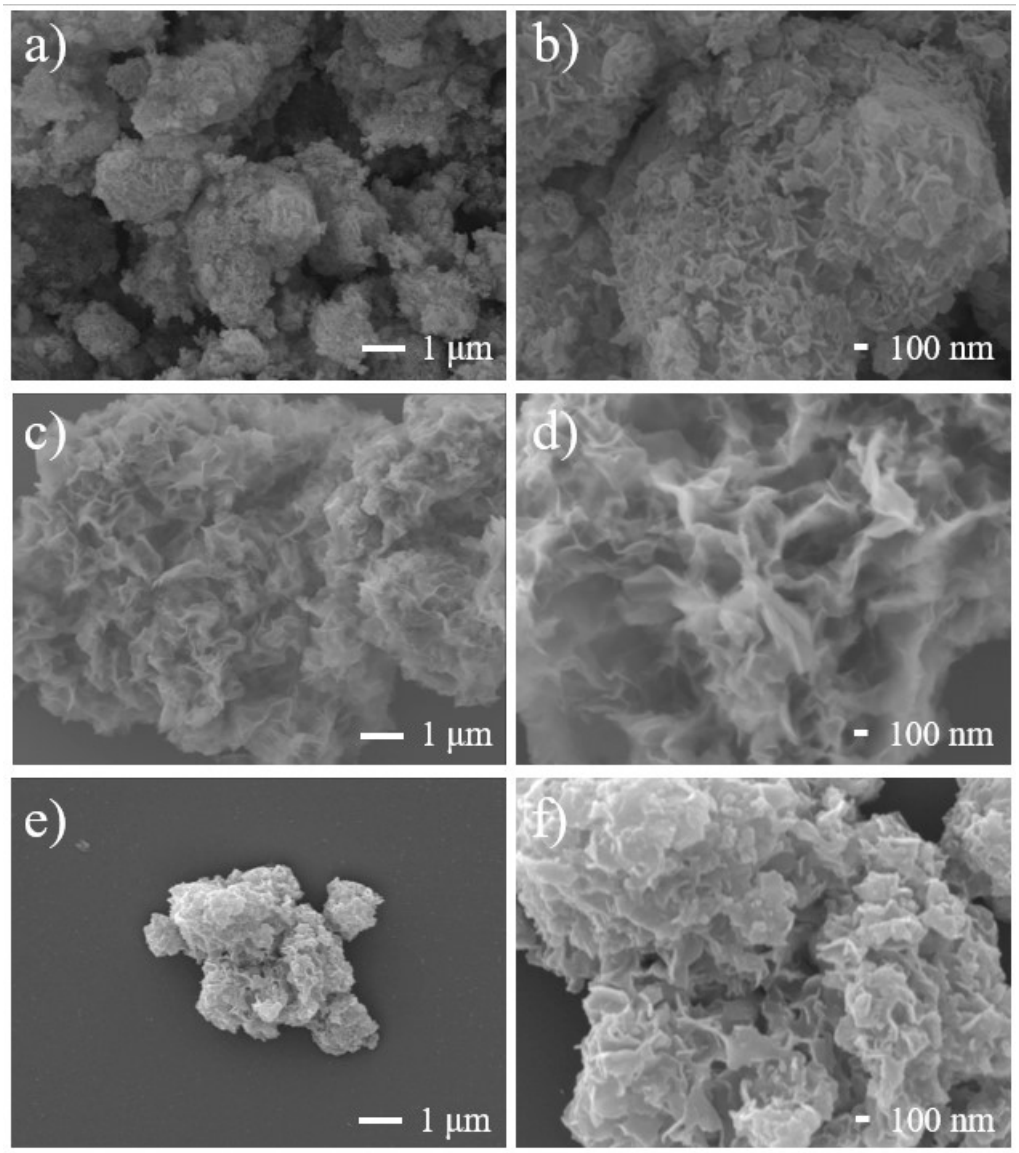

Fig. S4 The SEM images of Ni_2Co_1-S-140-*t*: (a-b) t = 1 h, (c-d) t = 6 h, (e-f) t = 12 h.

The Ni_2Co_1-S-140-6 sample, obtained after sulfidation at 140 ℃ for 6 h, exhibits the porous tremella-like structure, composed by large interlaced and fluffer nanosheets, while Ni_2Co_1-S-140-1 and Ni_2Co_1-S-140-12, generated after sulfidation at 140 ℃ for 1 and 12 h, respectively, show irregular spheres morphologies assembled by tightly packed nanosheets (Fig. S4). These results clarify that the morphologies of Ni_2Co_1-MOF derived sulfides are changed upon varying the sulfidation time, which probably influents the electrochemical performances of sulfides.

1.5.4 SEM images of Ni_2Co_1-S-T-6 (T = 100, 140, 180 ℃)

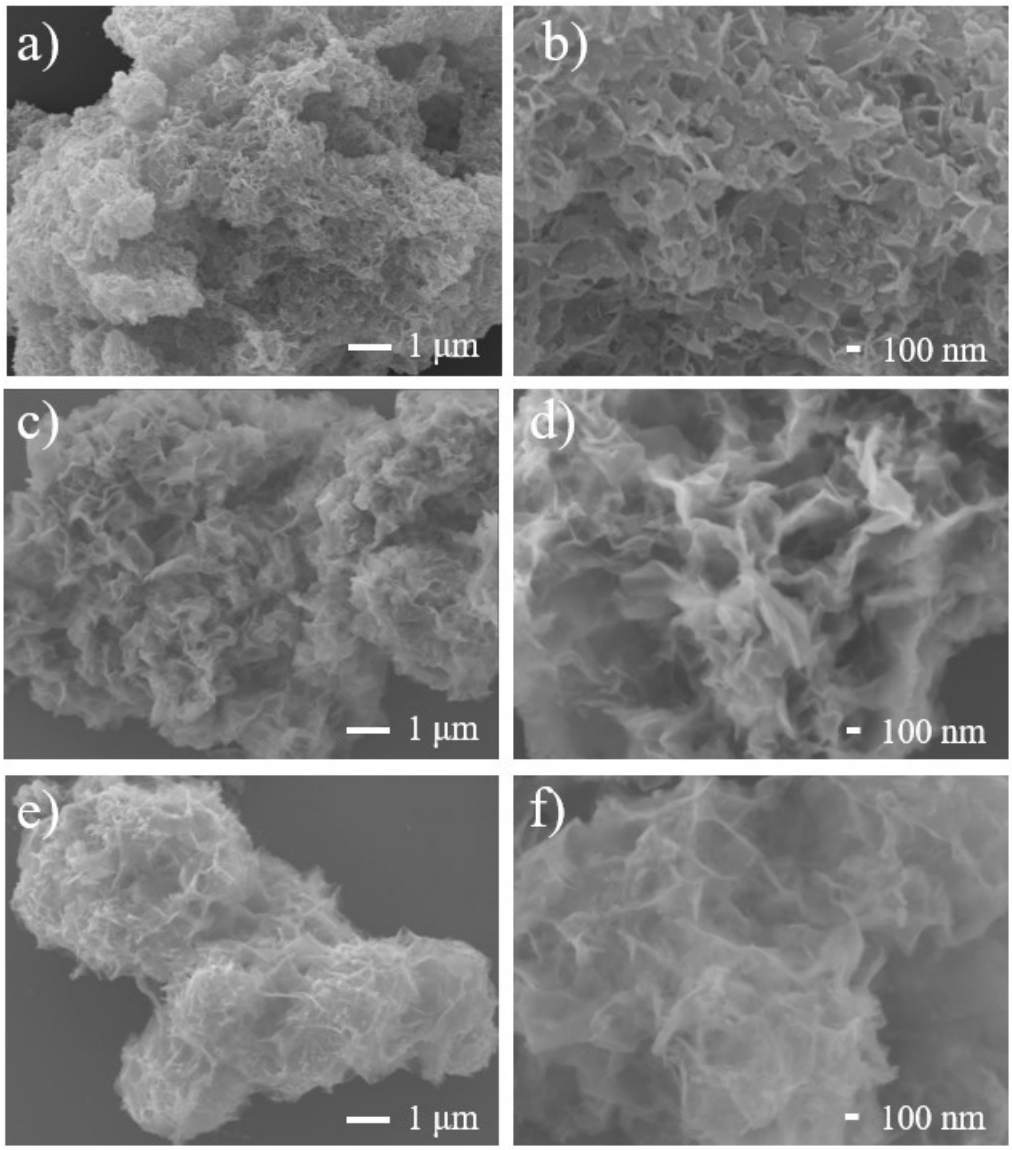

Fig. S5 The SEM images of Ni_2Co_1-S-*T*-6: (a-b) *T* = 100 ℃, (c-d) *T* =140 ℃, (e-f) *T* = 180 ℃.

Supplementary Fig. S5 shows the morphological evolution of Ni_2Co_1-S-*T*-6 materials upon sulfidation temperature (*T* = 100 ℃, 140 ℃ and 180 ℃). When the sulfidation temperature is 100 ℃, Ni_2Co_1-S-100-6 shows a metal foam-like morphology, composed of 2D nanosheets, while further increase the temperature up to 140 and 180 ℃, respectively, the morphologies of Ni_2Co_1-S-140-6 and Ni_2Co_1-S-180-6 are changed to the fresh-lettuce-like structures assembled by larger nanosheets. These results demonstrate that sulfidation temperature is also changed the morphology of Ni_2Co_1-MOF derived sulfides, which probably influents the electrochemical performances of sulfides.

1.6 TEM analysis

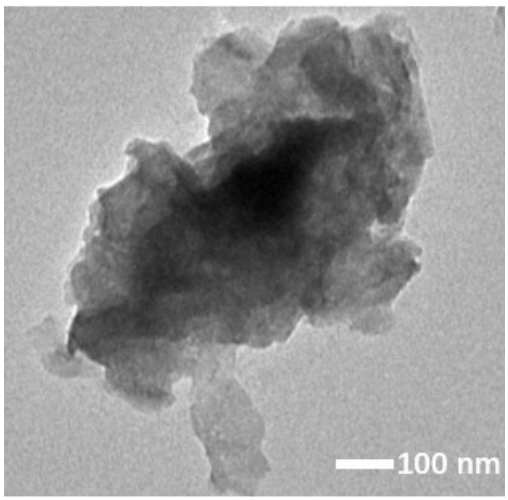

Fig. S6 The TEM image of Ni_2Co_1-S-140-6.

2.0 Electrochemical performance

2.1 GITT data of Ni_2Co_1-MOF, Ni_2Co_1-S, Ni_2Co_1-C, Ni_2Co_1-O, and Ni_2Co_1-OH

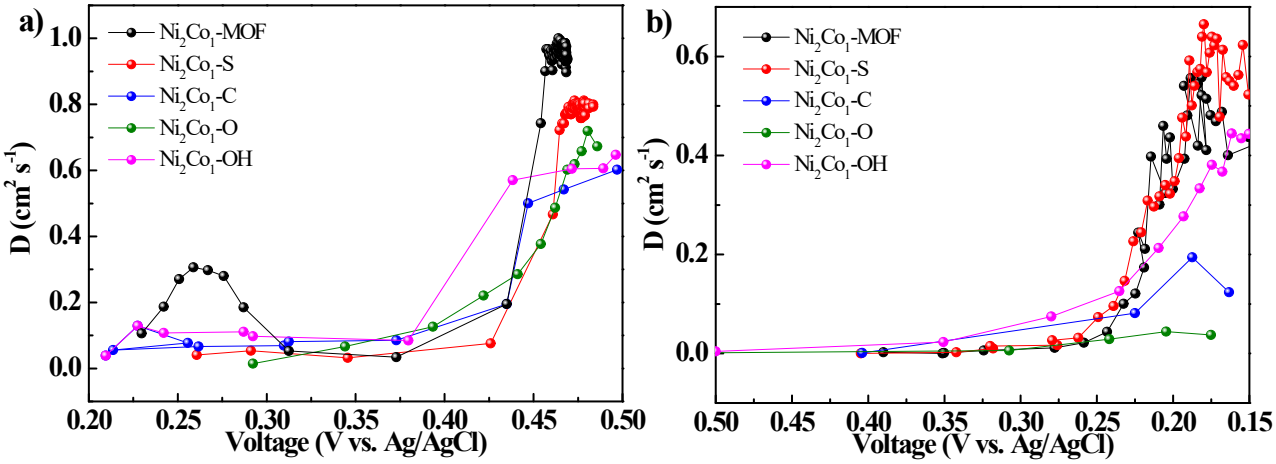

Fig. S7 The GITT curves of Ni_2Co_1-MOF, Ni_2Co_1-S, Ni_2Co_1-C, Ni_2Co_1-O, and Ni_2Co_1-OH at (a) charge process and (b) discharge process

2.2 Electrochemical performance of Ni_2Co_1-S-*T*-*t*

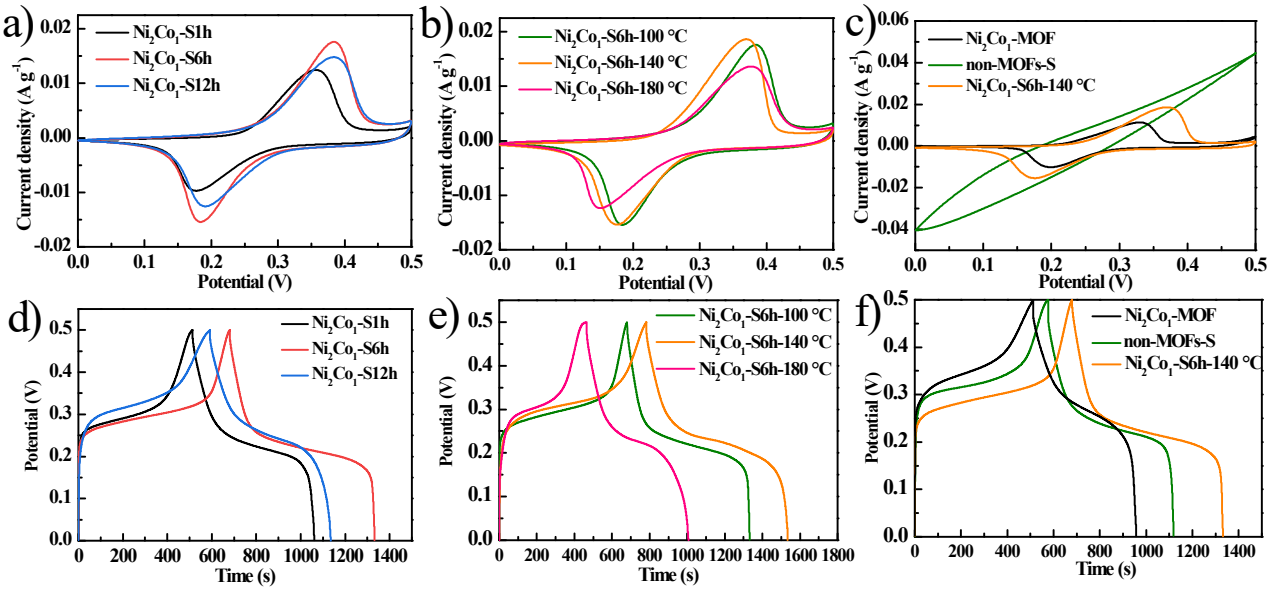

Fig. S8 The CV curves at 50 mV s^{-1} of (a) Ni_2Co_1-S-140-*t*, (b) Ni_2Co_1-S-*T*-6, (c) Ni_2Co_1-MOF, Ni_2Co_1-S-140-6 and the sulfide non-MOF-S, obtained sulfidation of the physical mixture of $Ni(NO_3)_2$ and $Co(NO_3)_2$. The GCD curves at 1 A g^{-1} of (d) Ni_2Co_1-S-140-*t*, (e) Ni_2Co_1-S-*T*-6, (f) Ni_2Co_1-MOF, Ni_2Co_1-S-140-6 and the sulfide non-MOF-S.

The detailed discussions about the comparison of Electrochemical performance of Ni_2Co_1-S-*T*-*t* have been described in the section of optimizing sulfidation parameters for boosting electrochemical performances of Ni_2Co_1-S-*T*-*t* materials of main text.

2.3 Electrochemical performance of PPy@AECC

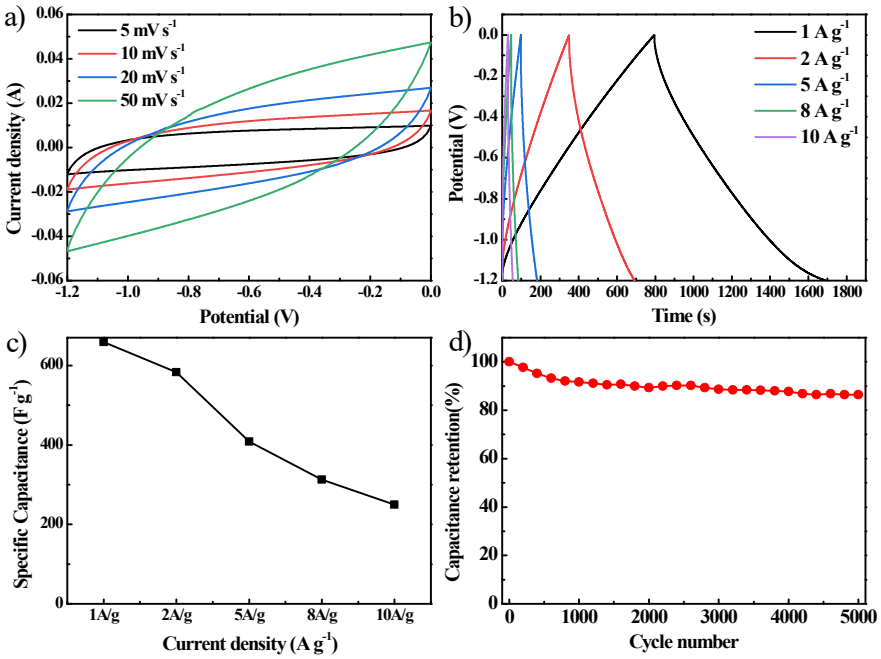

Fig. S9 Electrochemical performance of PPy@AECC tested in 1.0 M KOH: (a) CV curves at different scan rates ranging from 5 to 50 mV s^{-1}, (b) GCD curves at different discharge current densities ranging from 1 to 10 A g^{-1}, (c) the specific capacitances at various discharge current densities ranging from 1 to 10 A g^{-1}, (d) the plots of specific capacitances at 10 A g^{-1} over 5000 charge/discharge cycles.

For PPy@AECC negative electrode material, the potential windows for is −1.2 to 0 V in a three-electrode system (Fig. S9a), and the specific capacitance, calculated based on the imperfect symmetry GCD curves at 1 A g^{-1} is 659F g^{-1} (Fig. S9b), the rate capability when the discharge current densities ranging from 1 to 10 A g^{-1} is 37.9% (Fig. S9c), and the capacitance retention at 10 A g^{-1} is 86.4% after charge/discharge of 5000 cycles (Fig. S9d).

2.4 The Nyquist plots of Ni_2Co_1-S-140-6//PPy@AECC device

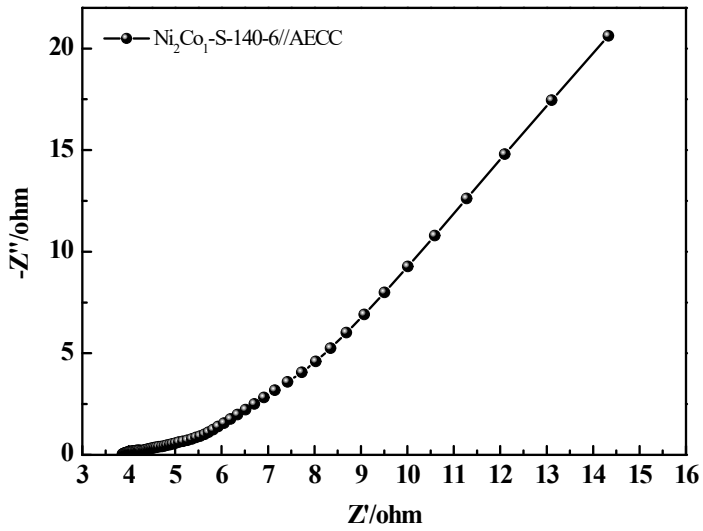

Fig. S10 The Nyquist plots of the fabricated Ni_2Co_1-S-140-6//PPy@AECC A-ASC device tested in 1 M KOH.

The Rs of Ni_2Co_1-S-140-6//PPy@AECC A-ASC device is 2.38 Ω, calculated based on the Nyquist plot (Fig. S10).

2.5 The Rct and Rs of Ni_xCo_y-MOF and Ni_2Co_1-MOF derivatives.

Table S4 The Rct and Rs of Ni_xCo_y-MOF and Ni_2Co_1-MOF derivatives.

	Rs (Ω)	Rct (Ω)		Rs (Ω)	Rct (Ω)
Ni-MOF	4.495	3.163	Ni-S-140-6	2.483	3.852
Ni_1Co_2-MOF	2.363	0.2416	Ni_1Co_2-S-140-6	3.801	1.828
Ni_1Co_1-MOF	2.866	0.5231	Ni_1Co_1-S-140-6	4.171	2.447
Ni_2Co_1-MOF	2.706	0.627	Co-S-140-6	2.427	0.1668
Co-MOF	5.448	0.7277	Ni_2Co_1-S-100-1	4.255	0.5463
Ni_2Co_1-S-140-6	3.162	0.8825	Ni_2Co_1-S-100-6	3.162	0.8825
Ni_2Co_1-C	4.687	0.496	Ni_2Co_1-S-100-12	3.229	0.8759
Ni_2Co_1-O	3.766	0.6918	Ni_2Co_1-S-100-6	4.255	0.9439
Ni_2Co_1-OH	3.868	0.1176	Ni_2Co_1-S-140-6	3.162	0.8825
Non-MOFs-S	4.251	1.328	Ni_2Co_1-S-180-6	4.49	1.058

As shown in Tab. S4, the Rct of bimetallic Ni_xCo_y-MOF (Ni_1Co_2-MOF: 0.2416 Ω; Ni_1Co_1-MOF: 0.5231 Ω and Ni_2Co_1-MOF: 0.627 Ω) were significantly lower than that of Ni-MOF (3.1630 Ω) and Co-MOF (0.7277 Ω), indicating that bimetallic Ni_xCo_y-MOF exhibit better good charge transfer capability compared with that of Ni-MOF and Co-MOF. The Rct values of Ni_2Co_1-S-140-6 (0.8825 Ω) and Ni_2Co_1-O (0.6918) are comparable to that of Ni_2Co_1-MOF, illuminating that the charge transfer capabilities of Ni_2Co_1-MOF almost maintain after sulfidation and oxidation. Ni_2Co_1-C (0.4960 Ω) and Ni_2Co_1-OH (0.1176 Ω) exhibit the lower Rct, compared to Ni_2Co_1-MOF, the charge transfer capabilities of Ni_2Co_1-MOF are slightly enhanced after carbonization and hydroxylation.

2.6 the electrochemical performance of the Ni_2Co_1-C-900

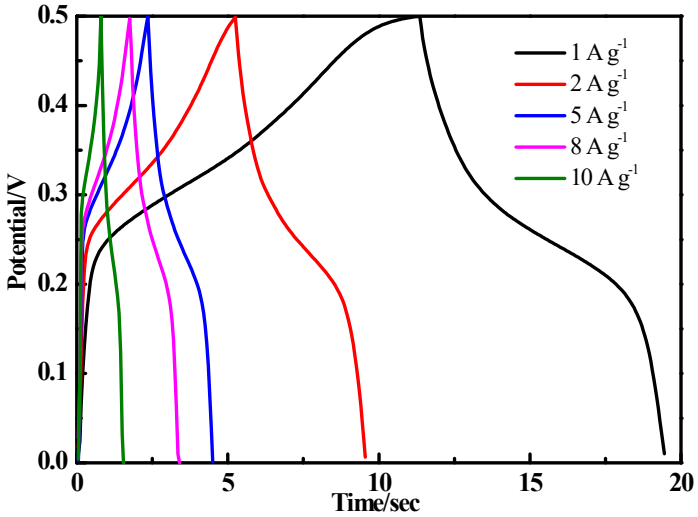

Fig. S11 GCD curves at different discharge current densities ranging from 1 to 10 A g^{-1} of Ni_2Co_1-C-900.

After elevating the carbonization temperature of Ni_2Co_1-MOF to 900 ℃, the GCD curves reveal that the specific capacitance of Ni_2Co_1-C-900 is comparable to that carbonized at Ni_2Co_1-C-600, indicating elevating carbonization temperature does not lead to high chemical performance of Ni_2Co_1-MOF carbonization derivative.

3.0 Supplementary References

1. Z. Fang, B. Bueken, D. E. De Vos and R. A. Fischer, Defect-Engineered Metal-Organic Frameworks, *Angew. Chem. Int. Ed.*, 2015, **54**, 7234-7254.
2. W. Xu, Y. Zhang, J. Wang, Y. Xu, L. Bian, Q. Ju, Y. Wang and Z. Fang, Defects engineering simultaneously enhances activity and recyclability of MOFs in selective hydrogenation of biomass, *Nat. Commun*, 2022, **13**, 2068.
3. W. Xu, K. B. Thapa, Q. Ju, Z. Fang and W. Huang, Heterogeneous catalysts based on mesoporous metal–organic frameworks, *Coordination Chemistry Reviews*, 2018, **373**, 199-232.
4. Z. Fang, J. P. Durholt, M. Kauer, W. Zhang, C. Lochenie, B. Jee, B. Albada, N. Metzler-Nolte, A. Poppl, B. Weber, M. Muhler, Y. Wang, R. Schmid and R. A. Fischer, Structural complexity in metal-organic frameworks: simultaneous modification of open metal sites and hierarchical porosity by systematic doping with defective linkers, *J Am Chem Soc*, 2014, **136**, 9627-9636.